Radiologic evaluation of pediatric hydrocephalus

Alp Dinçer · M. Memet Özek

Abstract

Introduction The aim of this review is to present the contemporary role of radiology in evaluating pediatric hydrocephalus. Although conventional brain imaging with ultrasound (US), computed tomography (CT), and magnetic resonance imaging (MRI) reveal the degree of ventricular enlargement and often the etiology of the hydrocephalus, the diagnosis and management of hydrocephalus present common problems in pediatric populations.

Discussion US, usually sufficient to assess and monitor ventricular size, is used most commonly in preterm infants who have germinal matrix hemorrhages and not able to tolerate transport to the radiology department. Although CT can demonstrate gross dilatation of ventricles, in most cases, it will be necessary to more closely define the nature of the obstruction, either functionally or anatomically. MRI is the best imaging modality to provide such functional and anatomic information. However, since identification of obstructive pathologic processes at any level through the cerebrospinal fluid (CSF) pathway in patients with hydrocephalus is of significant importance because it can change the treatment options, avoiding shunt insertion, a more sophisticated MRI approach is needed instead of obtaining a routine cranial MRI. Furthermore, the outcome after neuroendoscopic procedures is clearly related to patient selection under guidance of neuroimaging.

Conclusion Therefore, the article focuses mainly on the effective usage of various MRI sequences in both diagnosis and follow-up of pediatric hydrocephalus, such as 3D CISS, cine PC, TSE, and GRE T2* sequences, to be able to investigate all possible obstructive pathology through the CSF pathway and to assess the efficiency of treatment in a standardized way.

A. Dinçer
Department of Radiology, School of Medicine,
Acibadem University,
Inonu Cad. Okur Sok. No:21, Kozyatagı,
Istanbul 34742, Turkey

M. M. Özek
Division of Pediatric Neurosurgery, School of Medicine,
Acibadem University,
Inonu Cad. Okur Sok. No:21, Kozyatagı,
Istanbul 34742, Turkey

A. Dinçer (✉)
Department of Radiology, Acibadem Kozyatagi Hospital,
Inonu Cad. Okur Sok. No:21, Kozyatagı,
Istanbul 34742, Turkey
e-mail: alpdincer@yahoo.com

Introduction

Neuroimaging has been important for the diagnosis and management of hydrocephalus, beginning with pneumo-encephalography [21]. A number of different descriptions and radiologic classification schemes for hydrocephalus were proposed over the years [9, 16–18]. However, in the past, surgical therapy, irrespective of the classification, consisted of ventricular or lumbar cerebrospinal fluid (CSF) drainage to the right atrium or the peritoneal cavity. Therefore, the demand for imaging was usually limited

for the diagnosis of hydrocephalus, differentiating from ventriculomegaly, clarifying the etiology as much as we could, and uncovering the complications. However, the availability of different surgical treatment options necessitate the precise classification of hydrocephalus to be able to select the best treatment modality, avoiding shunt insertion, and to be able to compare results. Because our ultimate goal with imaging is to be able to predict the success of treatment before surgery and expand the indication of neuroendoscopic procedures, demonstrating the level of obstruction(s) has been a key issue. First of all, to achieve that goal, imaging modality should provide excellent imaging capability to demonstrate all possible obstructive pathological processes at any level through the CSF pathway from the ventricles to the cortical subarachnoid compartment [6, 17]. Magnetic resonance imaging (MRI) is the single and best imaging modality for covering all of the imaging demands, providing one-stop shopping. Besides anatomical information, it also may give information on CSF flow dynamics. No other investigation or combination of investigations will give as much detail as MRI. Although conventional T1-weighted and T2-weighted images have been used for the diagnosis and classification of hydrocephalus, it is far from being an ideal neuroimaging technique despite many improvements eliminating CSF and vascular flow artifacts. The disadvantages of conventional images when investigating cisternal anatomy are poor spatial resolution, poor contrast-to-noise ratio between the cisterns and neighboring structures, and CSF flow effects [6]. In the radiological studies with conventional MRI, the contribution of cisternal obstruction in the formation of hydrocephalus has been underestimated due to relative insensitivity of conventional MRI to the anatomical details of the basal cisterns. A few publications dealing with three-dimensional constructive interference in the steady state (3D CISS) pointed out the importance of the cisterns [1, 5–7, 13, 14]. Indeed, historical publications with old radiological techniques such as air pneumoencephalography, cisternography with contrast media, or radionuclide cisternography had already demonstrated the importance of the cisternal adhesion in terms of the classification of hydrocephalus [3, 8, 11]. So, it has been known that the presence and the severity of basal cisternal adhesions or obstructive membranes play an important role not only in the decision-making process in the treatment of hydrocephalus but also could be used to predict the success of the treatment modality [6, 15]. The lack of any reliable noninvasive test in the determination of the resorption capacity of the arachnoid granulations or brain capillaries increases the importance of imaging. In this review, we attempt to present the important and challenging role of radiological imaging in the current evaluation of pediatric hydrocephalus both in the preoperative and postoperative periods, emphasizing MRI.

Computed tomography

Computed tomography (CT) is the best means of obtaining images as it is easily available, fast, reliable, and compatible with standard life support devices. Different examination for follow-up can be easily compared. Children often do not have to be sedated with the modern fast scanner. The nature of the obstruction can be obvious with CT because of significant ventricular dilatation proximal to an obstruction, with normal-sized or even compressed distal ventricles, but not sufficient in detail. Therefore, in the era of the presence of modern treatment options for hydrocephalus, CT does not usually provide adequate information to meet all the necessities of the neurosurgeon. However, CT has been most commonly informative in patients with aqueduct stenosis and with dilatation of the lateral and third ventricles in conjunction with a normal-sized fourth ventricle and small subarachnoid space. Also, the isolated lateral ventricle and isolated fourth ventricle could be easily diagnosed using CT. Furthermore, follow-up of cases after shunt insertion is easily made with CT. The ventricle size decreases from shunt insertion to 12 months scan and then remains usually stable. Therefore, the 1-year follow-up scan is the most useful baseline for long-term follow-up. However, it is best to obtain a 3-month scan also because shunt failure is so common in the first year. In addition to that, these children need lifelong follow-up and investigation of shunt malfunction with CT [10, 22]. Therefore, ionizing radiation is the most important concern in the follow-up of the pediatric patient with shunt.

Ultrasound

Ultrasound (US) is useful to explore the brain and the ventricles in the first 12–18 months of life while the anterior fontanel is still open. It can be used as a bedside screening test. The size and shape of the lateral ventricles is easily visualized, but the size of the third and fourth ventricles is very difficult to assess by US. Therefore, the precise diagnosis and cause of hydrocephalus is rarely made by US alone. Furthermore, US is usually unable to show posterior fossa details and investigation for the aqueduct, the floor of the third ventricle, and the foramen magnum are mostly not reliable with it. Besides, the quality of the US image is user-dependent and the reproducibility of US is not high. The best indication for US is follow-up of ventricular dilatation before or after surgical treatment in the first 2 years of life, but in case treatment of ventriculome-

galy is indicated, other means of brain imaging should be obtained [22].

Magnetic resonance imaging

MRI is the examination of choice for showing dilatation of the ventricular system, differentiating the ventriculomegaly from hydrocephalus, and revealing the underlying cause. Conventional T1-weighted and T2-weighted sequences are used routinely. These are usually informative to demonstrate the pathologic signal intensities within brain parenchyma, to evaluate the size and the shape of the ventricles, and to show most of the space-occupying lesions both in intra-axial and extra-axial locations. These data were absolutely enough in the past when the shunt insertion was the only option in the treatment of hydrocephalus. Nowadays, to be able to appreciate the best treatment modality, including endoscopic procedures and shunt insertion, and to guide the surgical procedure, CSF pathways from the ventricles to the cortical subarachnoid

compartment and CSF flow at various sites should be carefully scrutinized in detail. To accomplish that, relatively new MRI sequences either alone or a combination of them should be obtained in conjunction with the conventional T1-weighted and T2-weighted images. Although various MR cisternographic and motion-sensitive MRI techniques (spin echo [SE], turbo spin echo [TSE], steady-state free precession [SSFP], three-dimensional constructive interference in the steady state [3D CISS], reverse fast imaging with steady-state precession [PSIF], spatial modulation of magnetization [SPAMM], and cine phase contrast [cine PC]) have been applied, 3D CISS or equivalents, TSE or FSE, and cine PC have gained wide acceptance in evaluating the CSF flow and/ or anatomy of the cisterns [5, 6].

Careful attention should be paid to be able to demonstrate the absence or presence hemorrhage and related membranes in the cisterns by using hemosiderin-sensitive sequences under the age of 2 years. Gradient echo (GRE) T2* or susceptibility weighted imaging (SWI) easily detect previous hemorrhage in the ventricles and cisterns (Fig. 1). In the presence of extensive susceptibility or blooming effect compatible with


Fig. 1 Axial TSE T2 weighted image (**a**) of a preterm infant with progressive head circumference at the age of 2 months presents mild to moderate hydrocephalus. There is no apparent clue for extensive hemorrhage, except a subtle hemorrhage on left atrial periventricular parenchyma. On the other hand, axial GRE T2* image (**b**) demonstrates extensive periventricular subependymal hemorrhage. Sagittal TSE T2 weighted image (**c**) shows Liliequist membrane and the cerebral aqueduct stenosis with inferior web. The basal cisterns seem to be clear on midsagittal TSE T2 weighted image, but midsagittal 3D CISS image (**d**) depicts prominent obstructive membranes in the prepontine cistern and thickened Liliequist membrane, which are not visible on conventional T1 and T2 weighted images
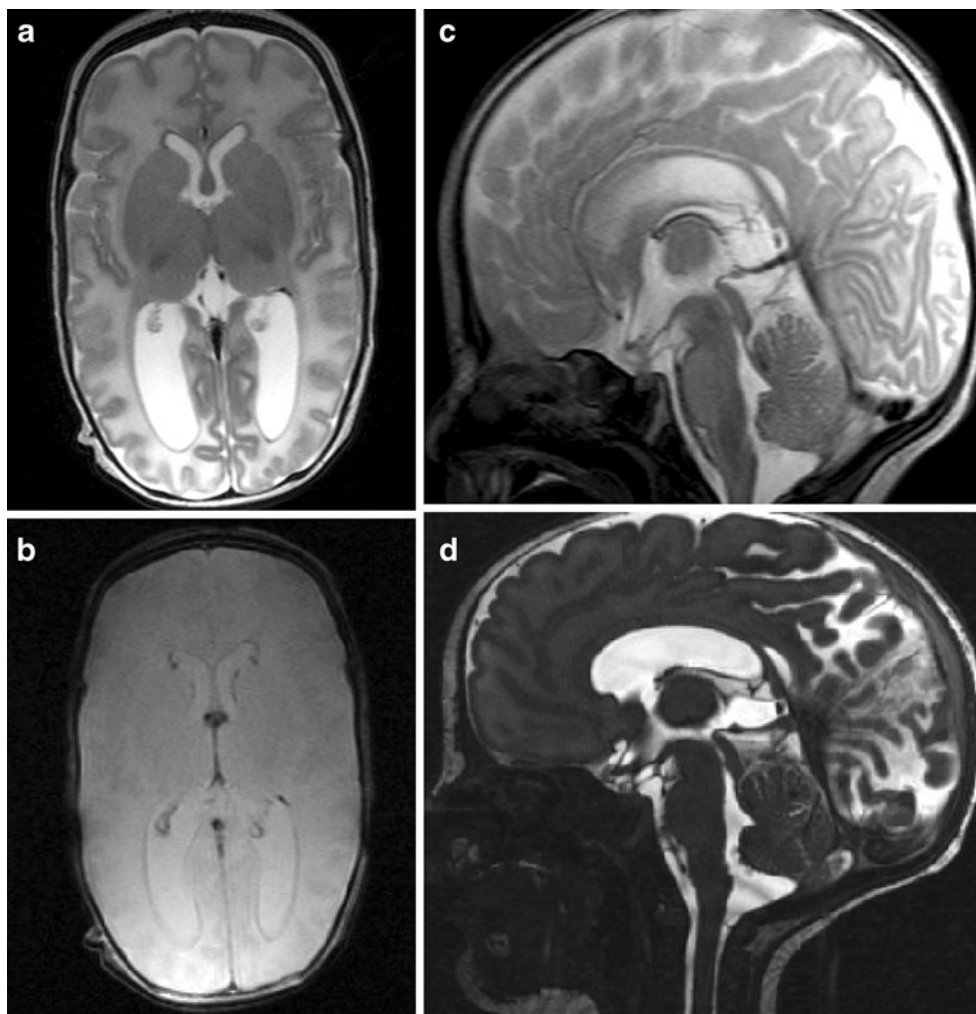
severe previous hemorrhage superimposed to basal cisterns and ventricles, shunt insertion may be the best alternative even if there is no direct sign of obstructive membranes in the cisterns or ventricles or both in 3D CISS sequence.

Three-dimensional constructive interference in the steady state

3D CISS is a fully balanced and inherently flow-compensated GRE sequence providing fine anatomic details about CSF pathways [1, 5–7, 14]. Two true-fast imaging with steady-state precession sequences with differing radiofrequency pulses are combined to produce strong T2/T1-weighted high-resolution 3D images. 3D CISS sequence combines the high signal-to-noise ratio with the extremely high spatial resolution and high CSF/brain tissue contrast. The value of this technique has been already demonstrated in hydrocephalus and the main advantage of 3D CISS has been not only demonstrating the fine anatomical details and membranes within the cistern, but also guiding the procedure and showing the location, number, and extent of the membranes [6] (Figs. 2 and 3). It is also useful to demonstrate membranes in the foramen of Monro, superior velum medullary synechia, the fourth ventricle outlet obstructions, and even intraventricle cystic mass not visible with conventional T1-weighted and T2-weighted images [6] (Figs. 4 and 5). We routinely obtain sagittal 3D CISS, covering the midsagittal structure, basal
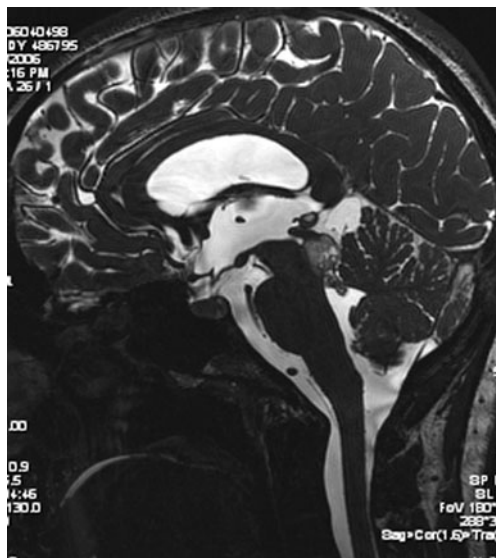

Fig. 2 Midsagittal 3D CISS nicely demonstrates all necessary information to be able to guide the neuroendoscopic surgery. The mass in the tectum (WHO grade 2 glioma), which obliterates the cerebral aqueduct, the floor of the third ventricle, the localization of tip of the basilar artery, the anatomy of the basal cisterns, and the width of the foramen of Monro (not shown), is exhibited
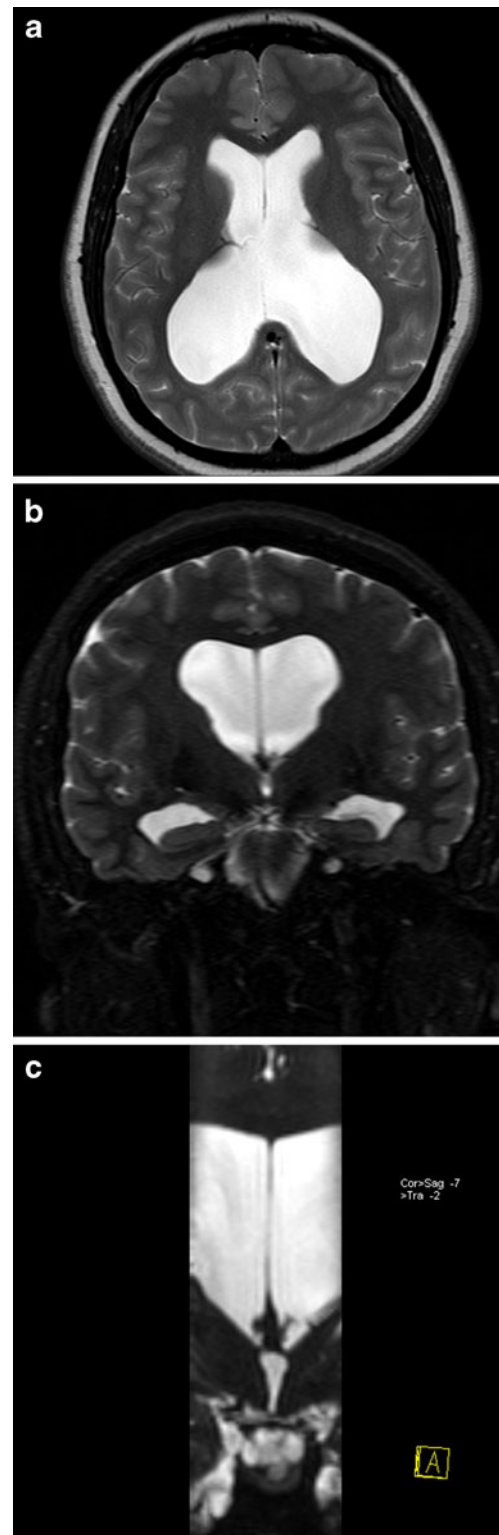
Fig. 3 An 8-year-old boy is admitted to the hospital due to headache. Axial TSE T2 weighted image through the lateral ventricles presents ventriculomegaly (**a**). Dilated temporal horns in the absence of perisylvian atrophy with a small-sized third ventricle are presented on coronal TSE T2 weighted image (**b**). Bilateral foramina of Monro seem to be open, but bilateral membranous obstructions of the foramina of Monro are shown on coronal oblique reformat image of sagittal 3D CISS (**c**)
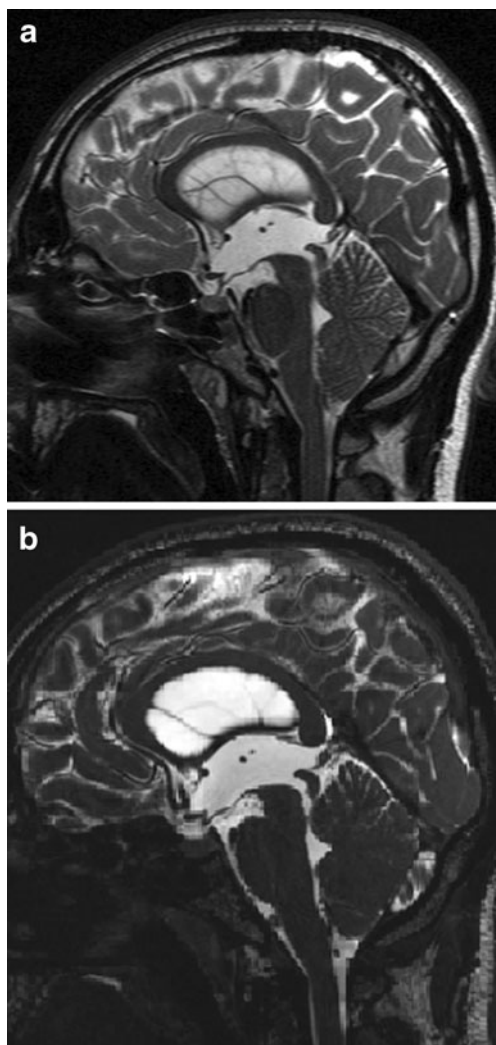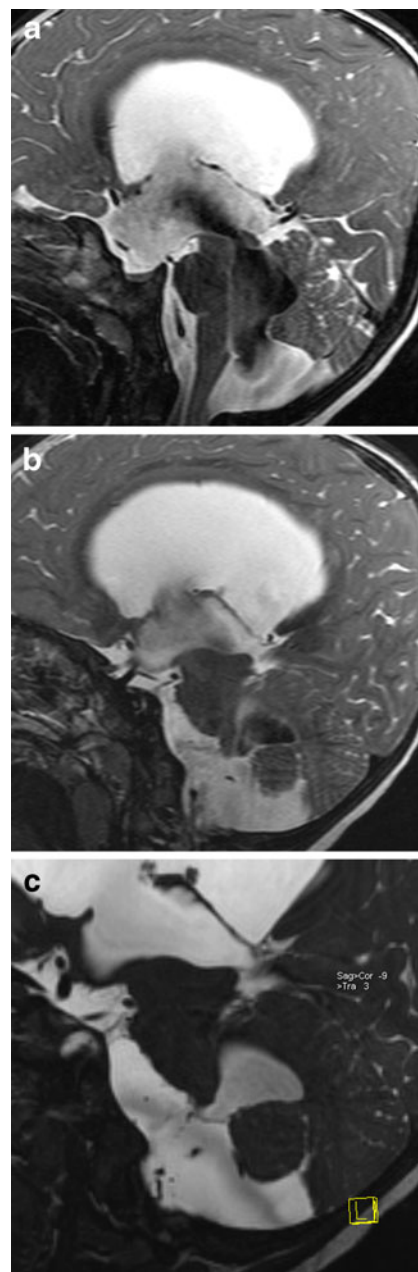
Fig. 4 Sagittal TSE T2 weighted image of an 18-year-old boy with headache demonstrates a moderate hydrocephalus with wide open cerebral aqueduct (**a**), but notice the lack of flow void phenomenon in the cerebral aqueduct compatible with an obstruction. Sagittal 3D CISS exhibited the velum medullary synechia (**b**)

cisterns, and fourth ventricle outlets with extremely high-resolution ($0.5 \times 0.5 \times 0.5$ or $0.6 \times 0.6 \times 0.6$ mm^3 at 3 T and $0.7 \times 0.7 \times 0.7$ mm^3 at 1.5 T) isometric voxel, which allows us to reconstruct in any arbitrary plane without losing any data. In conjunction with the investigation of the original sagittal source data, the real-time multiplanar volume reconstruction (MPVR) of the 3D CISS data give us an excellent chance to evaluate the membrane continuity both in the cisterns and the fourth ventricle outlets without any loss of image quality [4–6].

Because 3D CISS is a GRE sequence, it is more prone to artifacts. But, this is very rarely problematic. Lowering the flip angle to 50° instead of 70° and increasing the receiver bandwidth could help to eliminate aliasing and susceptibility artifacts. Other disadvantages of the 3D CISS sequence may be the relatively long scanning time and its poor tissue contrast

Fig. 5 Sagittal TSE T2 weighted image shows extensive flow voids in the cerebral aqueduct and foramen of Magendie and a huge third ventricle, simulating communicating hydrocephalus (**a**). Furthermore, the foramen of Luschka on the *left* seems to be open and there is no apparent membranous structure on the parasagittal TSE T2 weighted image (**b**). The signal intensity difference between the cistern and the fourth ventricle could be assessed as an indirect sign for obstructive membrane, but signal differences in or between cisterns and ventricles are common on TSE T2 weighted images due to CSF-related artifacts, which lower the specificity of this finding. However, parasagittal 3D CISS image (**c**) depicts the membranous structure which divides the cistern and the fourth ventricle

within the brain parenchyma. However, this technique is specially designed to show tissue/fluid distinction for which it is highly sensitive and specific.

Cine phase contrast

Cardiac-gated cine phase-contrast MRI is the only technique currently available to observe CSF flow noninvasively [5, 12, 20]. The phase-contrast technique provides "to and fro" CSF flow velocity and direction during a single cardiac cycle with specially designed flow-sensitive GRE sequence. This cardiac-gated phase-sensitive technique is based on the subtraction of two similar GRE images, one with flow-encoding gradients activated and one with identical parameters but without these gradients activated. The difference in phase between the subtracted images is due to motion along the particular gradient axis. The signal from the stationary tissues is almost completely eliminated. The sensitivity of the flow-encoding gradients must be set prospectively to prevent aliasing. Qualitative midline sagittal and quantitative axial image perpendicular to the imaging plane, mostly the aqueduct, must be acquired. It takes a maximum of 10 min to get both sequences with gating [5, 6]. Flow in the craniocaudal direction is encoded in shades of white; flow in the caudocranial direction is encoded in shades of black. Qualitative sagittal image is useful for demonstrating CSF motion at various points in the midline. It is very sensitive to demonstrate reduced or hyperdynamic flow. The high-resolution through plane axial quantitative technique is usually used to evaluate CSF motion through the aqueduct. It is simple to measure the mean and maximum velocities as well as the volumetric flow rate as a function of cardiac cycle. Integrating the volumetric flow rate over time permits the calculation of an aqueductal CSF "stroke volume." CSF flow is driven by expansion of the arteries during cardiac systole. When the volume of arteries increases during systole, the expansion of the volume leads to expulsion of the CSF from periphery of the brain towards the basal cisterns and the foramen magnum. The ventricular CSF is expelled from the ventricles towards the foramen of Monro, the fourth ventricle, and the posterior fossa. During diastole, the phenomenon is reversed and most of the flow ascending to the foramen magnum refilling the subarachnoid spaces from the reservoir accumulated in the spinal canal during systole. Through the cerebral aqueduct, the flow refills the lateral ventricles. In obstructive hydrocephalus, this technique is the first and, so far, the only method by which the absence of flow in a given structure can be objectively assessed. Unilateral atresia of the foramen Monro and the aqueduct stenosis could be easily confirmed. But, the analysis of flow is more difficult in the foramen magnum as this region is more complex [20].

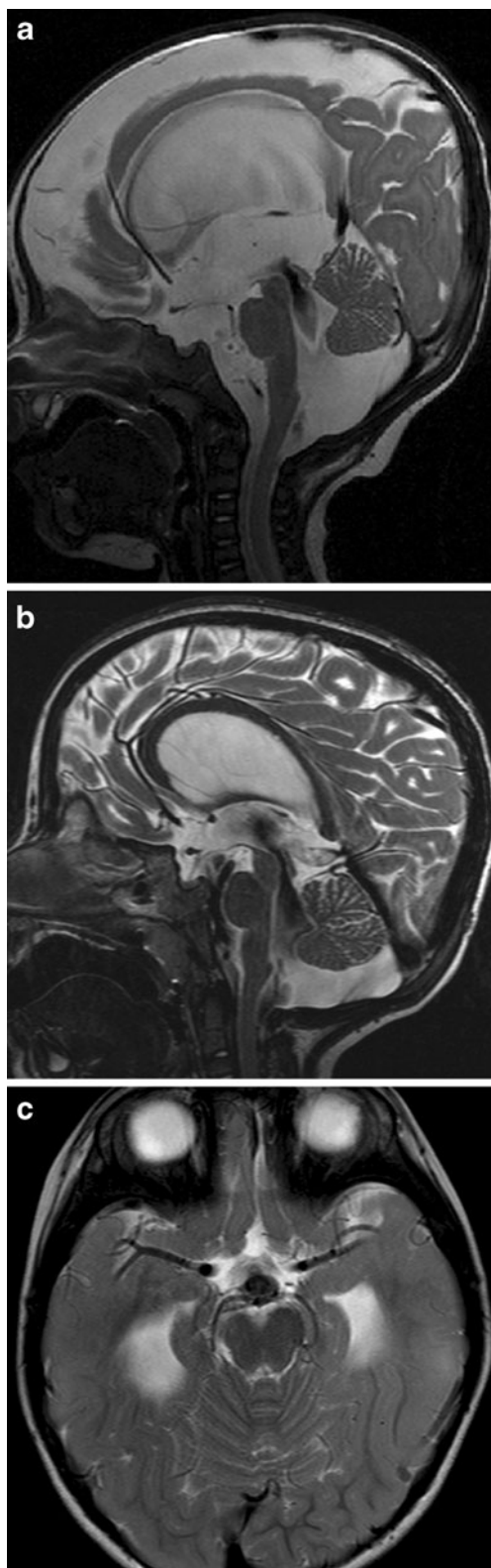Although cine PC is capable of showing flow as well as quantifying it, there are several disadvantages. To prevent aliasing artifact, which could affect the quality of both qualitative and quantitative assessments of cine PC, the strength of the velocity-encoding gradient should be set properly before scanning. On the other hand, cine PC demonstrates only bidirectional flow in a selected direction. It is possible to obtain multiple cine PC sequences in different anatomic locations and imaging planes, but not practical [6]. Whereas cine PC shows CSF flow, it is unable to demonstrate cisternal anatomic details and should be used in conjunction with 3D CISS. Furthermore, this technique is limited because of poor visualization of turbulent flow and the inability to measure bulk flow [20].

Turbo spin echo

The fast and widely available TSE sequence has been the basic MRI sequence since its description. However, TSE is more prone to flow-related artifact and its clinical application requires careful attention to the selection of imaging parameters. Moving protons cause signal loss, which is called "flow void" [5] (Figs. 5a and 6). Some strategies have been introduced to suppress or enhance the flow-related artifact and flow void in TSE sequence such as flow compensation and implementation of presaturation pulse. Also, some operator-dependent sequence parameters such as time of echo, slice thickness, spatial resolution, receiver bandwidth, the number of average, and echo train length could affect the flow-related artifact or flow void phenomenon [5]. It is proved that the section thickness and imaging planes are the most effective operator-dependent parameters of TSE sequences, as the thinner the slice, the more enhanced the visibility of the flow void [5]. Standard axial 5-mm TSE T2 weighted image is an exception, with high sensitivity to flow void. This could be explained by the perpendicularity between the flow direction and the imaging plane. Unfortunately, the axial imaging plane also enhances every kind of flow-related artifact in the cisterns, as well as flow through the fenestration, resulting in a decreased specificity.

Our MRI technique

A complete conventional study including axial TSE T1 weighted image, GRE T2*, diffusion-weighted imaging, axial, sagittal, and coronal TSE T2 weighted image, sagittal 3D turbo fast low-angle shot (TurboFLASH) T1, and sagittal 3D CISS followed by sagittal and axial–oblique cine PC are obtained for all pediatric patients with hydrocephalus [4–6]. The sagittal 3D CISS sequence was acquired with $0.6 \times 0.6 \times 0.6$-mm^3

isometric voxel, allowing reconstruction in any arbitrary plane for optimal visualization. If needed, axial TSE T1 weighted image and sagittal 3D TurboFLASH T1 were repeated after contrast administration. 3D CISS sequence was applied in the sagittal plane to cover the entire ventricular region and the fourth ventricular exits. Midline high-resolution sagittal cine PC was obtained for all patients as a standard sequence. The sequence parameters were as follows: TR, 37 ms; TE, 5.6 ms; averages, 3; FOV, 216 240 mm; section thickness, 2 mm; FA,
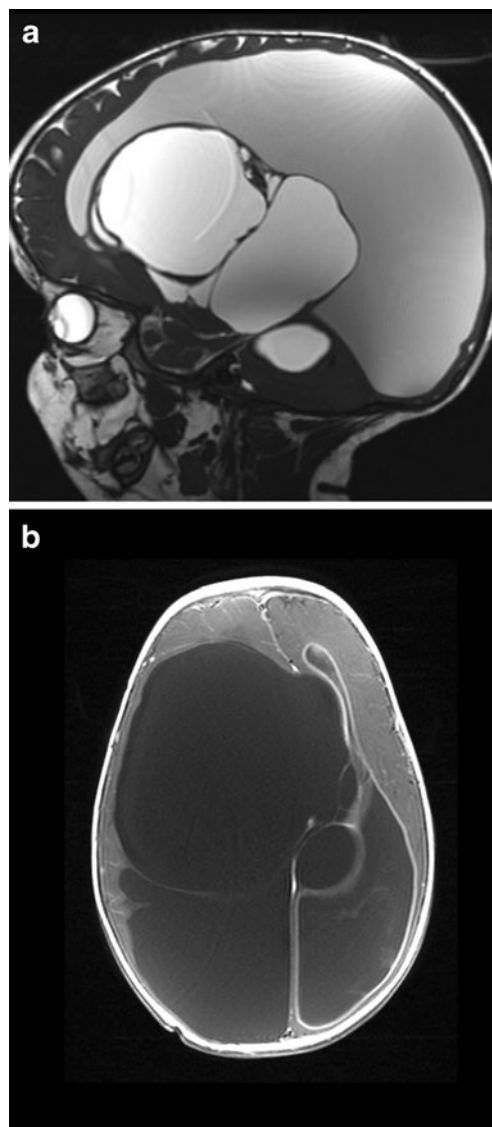
Fig. 7 Parasagittal 3D CISS exhibits a multicompartmental hydrocephalus (**a**). There are also signal intensity differences between the compartments, indicating different fluid content, which could be sign for infection. There is contrast enhancement on the periventricular ependymal lining, compatible with infection on post-gadolinium axial TSE T1 weighted image (**b**). Notice that only the left lateral ventricle wall enhances

Fig. 6 Sagittal TSE T2 (**a**, **b**) and axial TSE T2 (**c**) weighted images demonstrate the different degrees of the flow void sign through the cerebral aqueduct

Fig. 8 Midsagittal 3D CISS image (**a**–**c**) exhibits variability of the third ventricle anatomy. In **a**, a normal third ventricle of a patient with cerebral atrophy is presented. In **b**, the appearance of the third ventricle in moderate communicating hydrocephalus is shown. The cerebral aqueduct and fourth ventricle outlets are open and the cisterns are clear without any evidence of obstruction, but, in **c**, there is severe hydrocephalus with ballooning of the third ventricle. The cerebral aqueduct is open, but the fourth ventricle is obliterated with so-called hamartomas of neurofibromatosis type 1
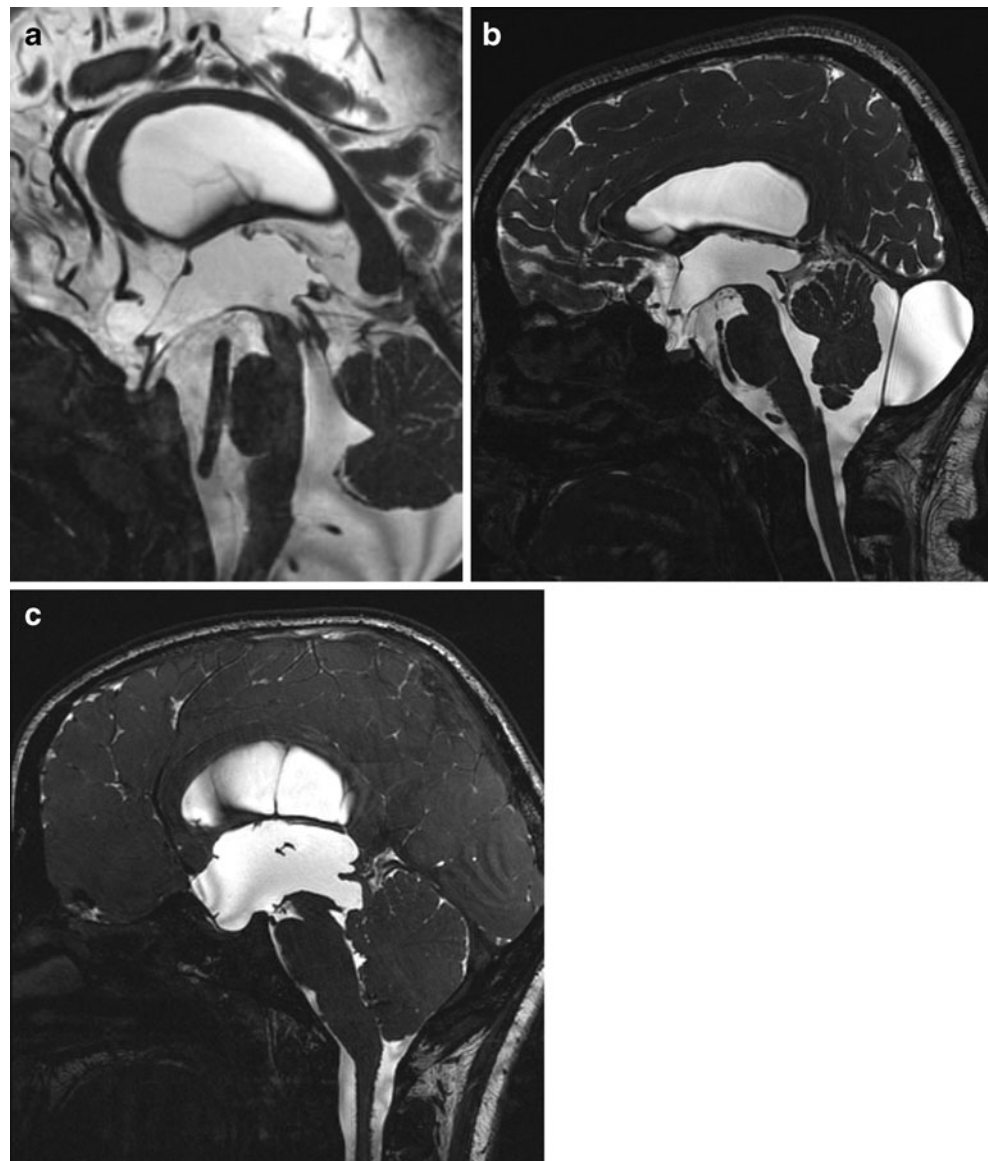
30°; matrix, 256×256; voxel size, 0.9×0.9×2 mm^3; velocity encoding, 20 cm/s; direction of flow encoding, foot to head; and bandwidth, 391 Hz/pixel. Electrocardiogram or pulse trigger was used with a 90% acquisition window. Just after acquisition, magnitude images, rephrased images, and phase images were reconstructed immediately. According to the anatomic region, the axial–oblique cine PC was obtained with the same parameters, except for the velocity-encoding direction, which was set to the through plane. In selected patients, if needed, cine PC was evaluated with vendor-supplied commercially available software.

Volumetric GRE T1-weighted images, such as Turbo-FLASH T1, are used to investigate associated anomalies and malformations of cortical development. GRE T2* or

SWI is routinely obtained to scrutinize hemorrhage within cisterns and/or ventricles in patients under the age of 2 years (Fig. 1b).

In addition to the space-occupying lesions, except arachnoid cysts, all patients with multicompartmental hydrocephalus or cyst, which has different signal intensity from CSF, should be given intravenous gadolinium to rule out infection (Fig. 7).

Our diagnostic criterion for obstructive membranes depends on demonstration of the membrane itself. Only membranes that could be followed all the way and divided the anatomic region completely into two or more parts are accepted as obstructive membranes. The nonobstructive membranes, which are normal cisternal
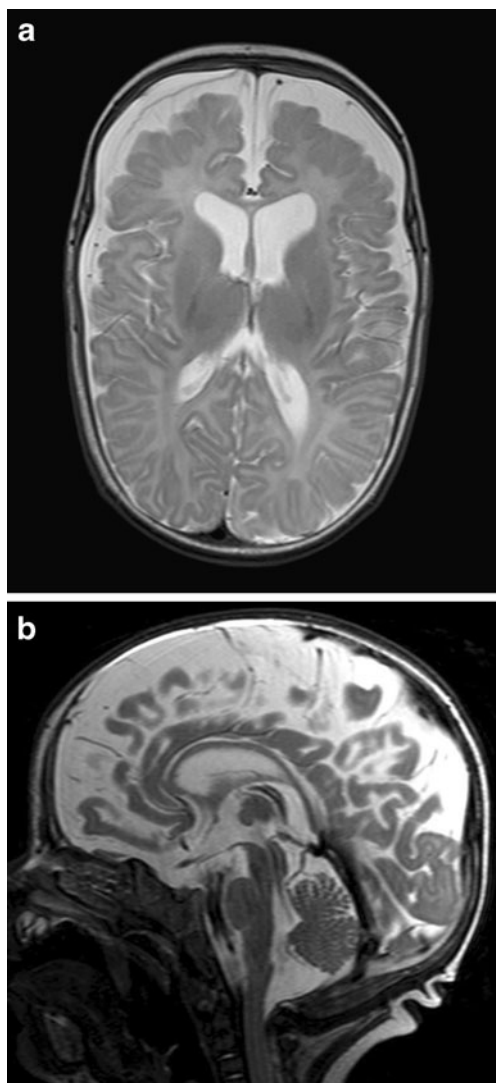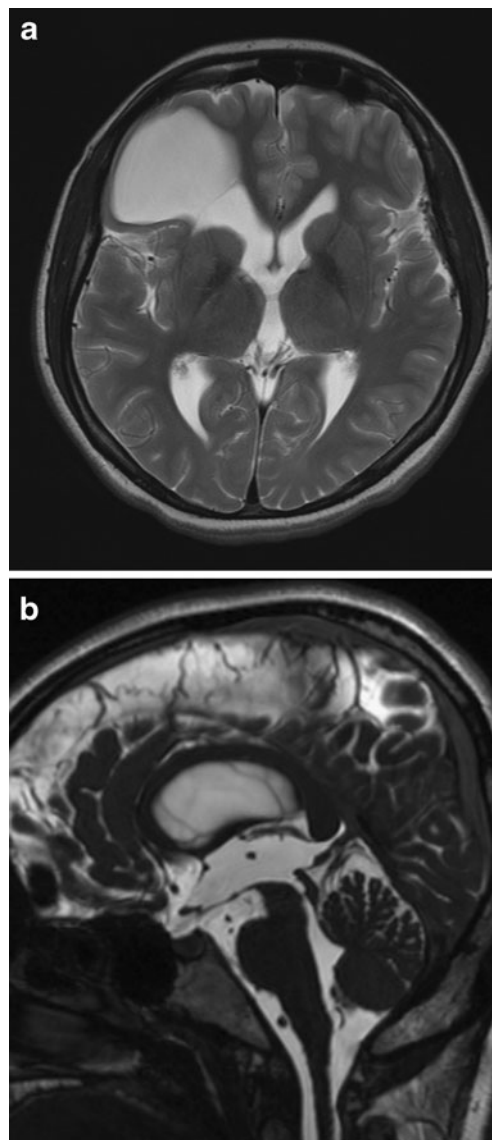
Fig. 9 Axial TSE T2 weighted image (**a**) of a 24-month-old patient with head enlargement over 95% indicates an increase in size of ventricles and subarachnoid space. Sagittal TSE T2 weighted image (**b**) demonstrates a normal-appearing third ventricle, the cerebral aqueduct, and cisterns. The patient is diagnosed as benign subarachnoid space enlargement of infancy with a family history

Imaging characteristics of hydrocephalus with CT and MRI

Simply stated, the diagnosis of hydrocephalus with CT and MRI is made when the ventricles are enlarged in the absence of cerebral atrophy. However, the differentiation of ventriculomegaly secondary to hydrocephalus and the resulting white matter atrophy is not always easy in the pediatric population. Enlargement of the recesses of the

structures such as Liliequist membrane, could be visible with high-resolution cisternal imaging, and these normal structures should not be taken into consideration as obstructive membranes. Signal intensity differences within cisterns or ventricles are not treated as a primary finding for making a decision as to the existence of an obstructive membrane. A sharp, linear zone of a transition signal intensity difference between two sides of the obstructive membrane is considered as only a complementary finding.

Fig. 10 Axial TSE T2 weighted image (**a**) demonstrates a large cystic cavity compatible with porencephalic cyst occupying a majority of the right frontal lobes. The medial aspect communicates with the right frontal horn. There is little brain parenchyma adjacent to the cyst in the right frontal lobe. However, sagittal 3D CISS (**b**) exhibits an enlargement in the third ventricle and a stenosis in the cerebral aqueduct. So, triventricular obstructive hydrocephalus is diagnosed in conjunction with the porencephalic cyst
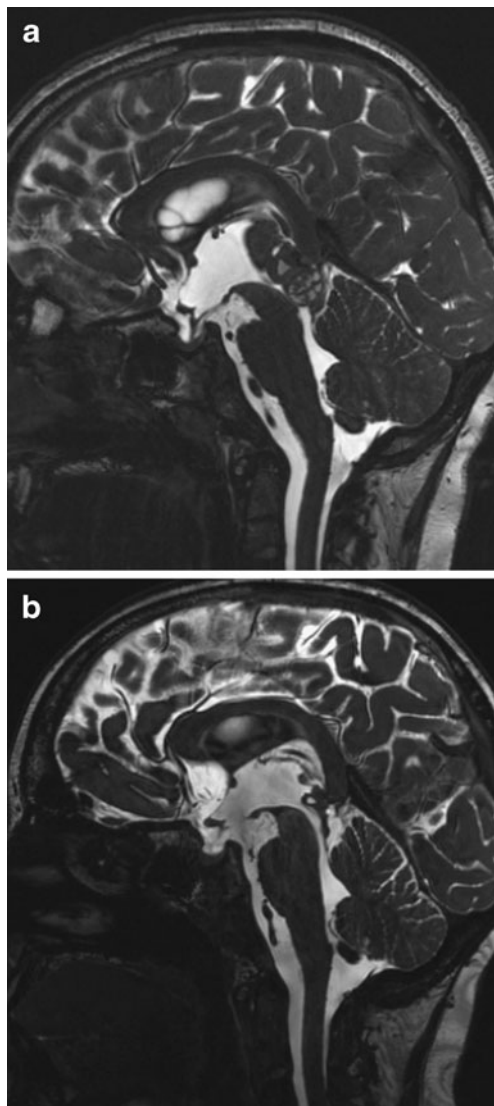
Fig. 11 WHO grade IV germ cell tumor of pineal gland obliterates the posterior part of the third ventricle causing triventricular hydrocephalus (**a**). After ETV and medical treatment, the tumor disappeared at 4-month follow-up and ventriculostomy fenestration is open and functional. Note that the size of the third ventricle is diminished (**b**)

third ventricle, dilatation of the temporal horn in the absence of perisylvian atrophy, symmetric periventricular interstitial edema, effacement of cortical sulci, absence of CSF flow void phenomenon, and stretching, thinning, and displacement of the corpus callosum are the basic imaging findings to make this differentiation. Narrowing of the mamillopontine distance, narrowing of the ventricular angle, widening of the frontal horn radius, and increase in ventricular index are the less reliable secondary findings.

Enlargement of the recesses of the third ventricle

It is the most reliable sign in the differentiation of hydrocephalus from the ventricular enlargement of white

matter atrophy (Fig. 8). The chiasmal and infundibular recesses seem to enlarge earlier and more severely than the suprapineal recesses. The assessment of the shape and size of anterior part of third ventricle in midsagittal high-resolution images is of particular importance. The anterior wall of the third ventricle becomes straightened and the floor of the third ventricle becomes straightened or convex downwards on sagittal images. Consequently, the mamillo-pontine distance is decreased by downwards displacement of the floor of the third ventricle.

Dilatation of the temporal horn

Another reliable sign of hydrocephalus is disproportional dilatation of the temporal horn. The configuration of temporal horn enlargement is characteristic in both the coronal and axial planes. The hippocampus is compressed and displaced inferomedially, and the choroidal fissure is usually enlarged. Temporal horns dilate less than the bodies of the lateral ventricles in patients with cerebral atrophy. The sylvian fissures should always be studied to assess the degree of temporal lobe atrophy before enlargement of the temporal horn is used to make a diagnosis of hydrocephalus. If the sylvian fissures are enlarged, enlarged temporal horns are not a reliable sign of hydrocephalus.

Periventricular interstitial edema

When pressure within the ventricular system is increased, normal centripetal bulk flow of CSF into the ventricular system reverses. Pressure gradients force intraventricular CSF into the extracellular spaces of the brain through the ependymal lining of the ventricles. The CSF flows through to brain parenchyma to sites of CSF absorptions. The consequent increased water within the cerebral parenchyma can be detected both by CT and MRI. On CT, it appears as hypodensity in the periventricular region and ventricular lining becomes indistinct. On MRI, there is a hyperintense rim surrounding the lateral ventricles in the fluid attenuated inversion recovery (FLAIR) or proton density images.

Effacement of cortical sulci

Enlargement of the ventricular system to a degree that is disproportionate to the enlargement of the cortical sulci may be an indicator of hydrocephalus. However, in pediatric patients, this parameter is often misleading because both atrophy and hydrocephalus can enlarge both the ventricles and sulci. Also, the size of the ventricles and subarachnoid spaces is variable over the first 2 years of life. Knowledge of the head size of the infant is essential; a large head or too rapidly enlarging head suggests hydrocephalus, whereas a small or diminishing head circumference is more compatible with atrophy (Fig. 9).

Fig. 12 A large suprasellar arachnoid cyst obliterating the third ventricle and causing hydrocephalus is seen on sagittal 3D CISS (**a**). At 6-month follow-up, flow void phenomenon on sagittal TSE T2 weighted image is detected both on the proximal and distal fenestrations compatible with functional stoma (**b**). Note that size of the third ventricle. Sagittal cine PC obtained at both systole (**c**) and diastole (**d**) confirm the free flow from the third ventricle to the cistern
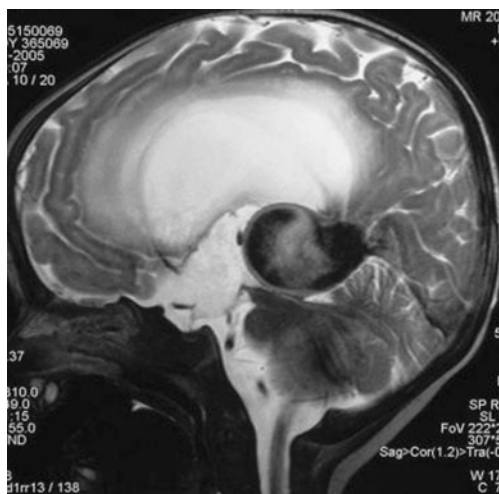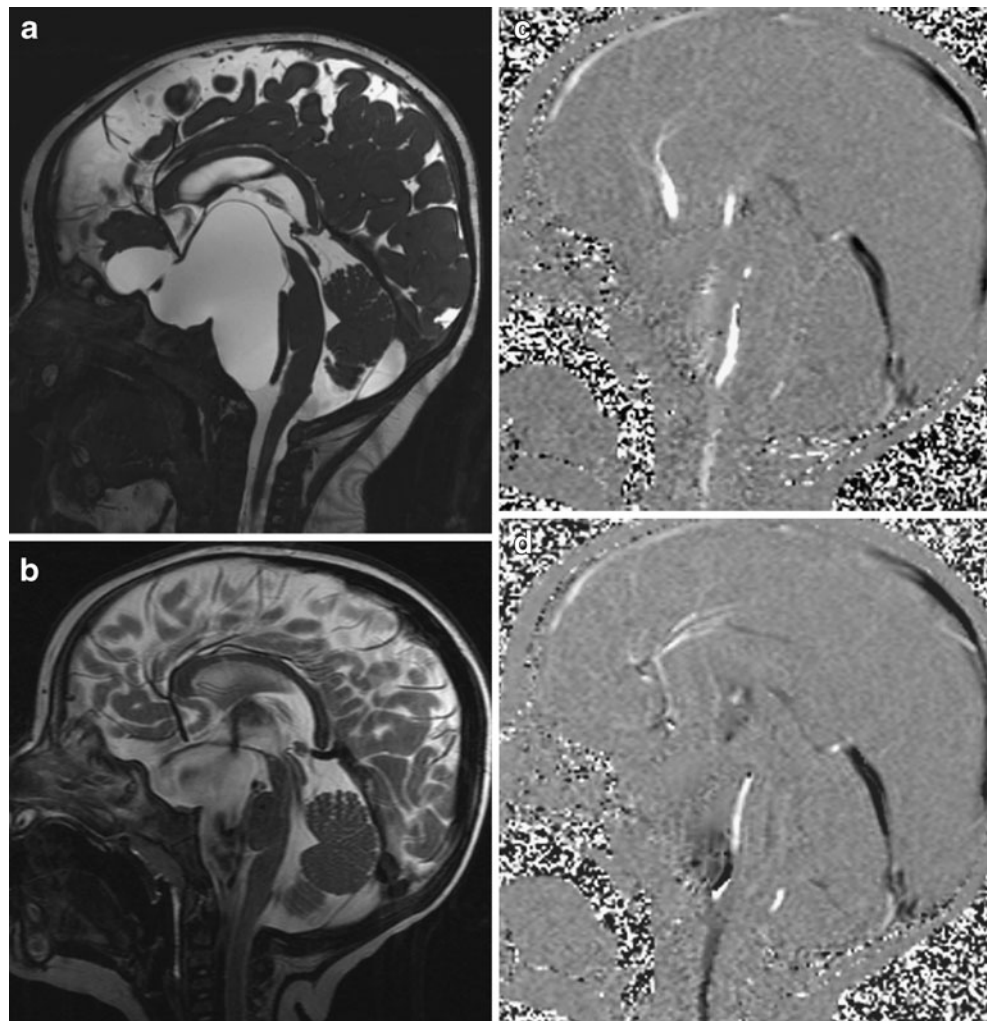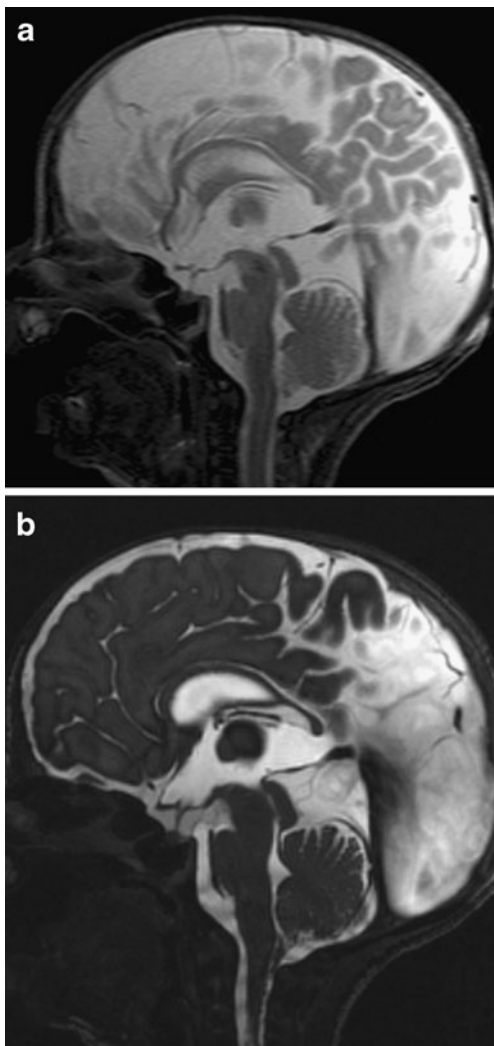

Fig. 13 Vein of Galen aneurysm compressing the cerebral aqueduct and causing a triventricular hydrocephalus is seen on midsagittal TSE T2 weighted image
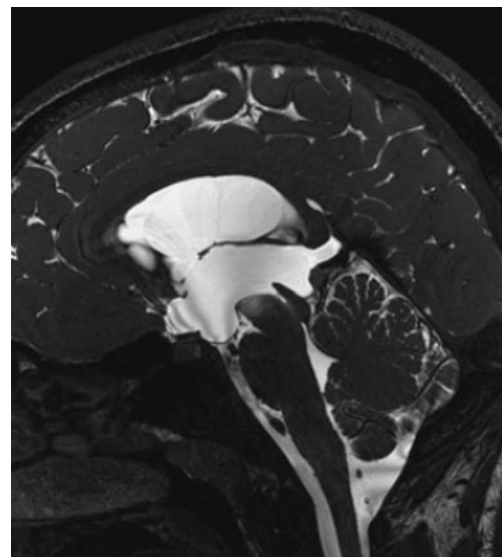
Fig. 14 A progressive craniocaudal narrowing in long tubular type of the cerebral aqueduct is seen in a patient with aqueduct stenosis on sagittal 3D CISS
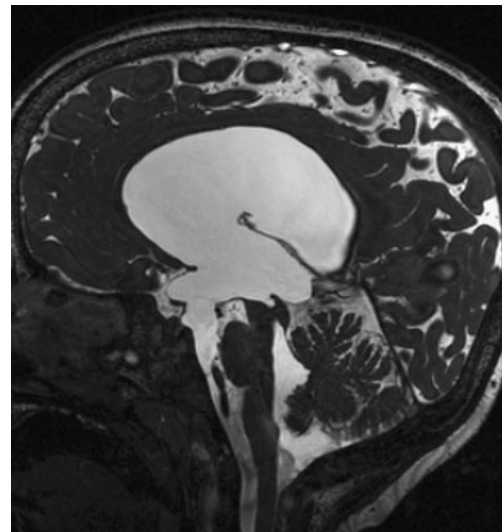
Fig. 15 There is a uniform narrowing in the cerebral aqueduct of an infant. Sagittal TSE T2 weighted image (**a**) demonstrates the lack of flow void in the cerebral aqueduct. Also, 3D CISS image (**b**) indicates the leaflets of Liliequist membrane

Fig. 16 The cerebral aqueduct is obliterated in the middle. A stoma on the third ventricle floor is also seen

Obstruction sites in the CSF pathway

Foramen of Monro

Obstruction of the foramen of Monro causes unilateral hydrocephalus. It is frequent and membrane, cyst, or tumor may be the causative agent. While conventional T1-weighted and T2-weighted images are usually enough to make a diagnosis of tumor, 3D CISS easily demonstrates obstructive membranes, small arachnoid, or choroid plexus cysts (Figs. 3

CSF "flow void" phenomenon

Flow void is the occurrence of a low signal in regions of flow [5]. For a SE or TSE sequence, this is caused in part by a lack of refocusing of moving protons, which is excited by the 90° pulse but not by the 180° pulse. For a GRE sequence, this is caused mostly by the intravoxel dephasing of protons. The flow void is usually a normal physiologic phenomenon. While its absence is usually indicative of an obstructive lesion, the demonstration of flow void means a functional stoma [5]. T2-weighted image obtained with TSE sequence is the best choice to investigate CSF flow void. But, as mentioned earlier, CSF flow void is strongly dependent on slice thickness and imaging plane of TSE sequence [5].
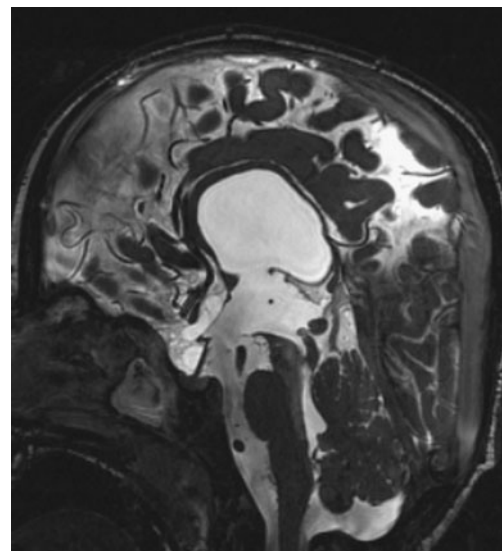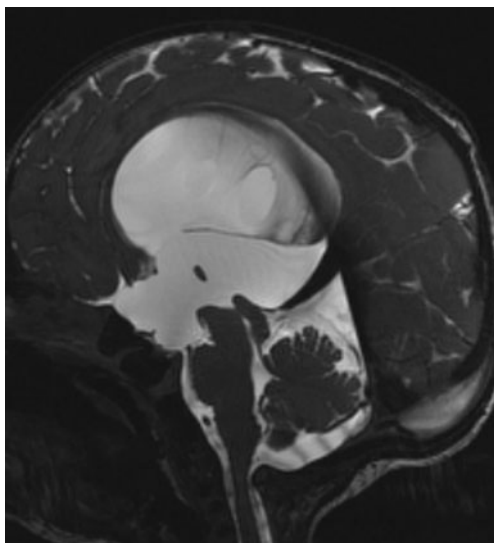

Fig. 17 Distal narrowing and proximal dilatation of the cerebral aqueduct are seen on midsagittal 3D CISS image

Fig. 18 Proximal narrowing in the cerebral aqueduct is demonstrated on midsagittal 3D CISS

and 5). Cine PC could be used to confirm the obstructive nature of the causative agent. Differentiating between the unilateral ventriculomegaly and unilateral hydrocephalus with conventional sequences could be difficult in some cases when there is no pathologic signal in the adjacent brain parenchyma (Fig. 10). But, demonstration of the open foramen of Monro by MRI cisternography is diagnostic in these cases. Bilateral foramen of Monro obliteration is extremely rare. Dilatation of the lateral ventricles in conjunction with a small-sized third ventricle is a rule. 3D CISS demonstrates the obstruction and the cause (Fig. 3).

Third ventricle

Hydrocephalus due to third ventricle obstruction is not common. Complete obstruction of the third ventricle by a mass, such as optic pathway glioma, suprasellar arachnoid cyst, craniopharyngiomas, vein of Galen aneurysm, and pineal gland tumor, is rare, but not the exception (Figs. 11, 12, and 13). The diagnosis of obstructive tumor in the third ventricle is straightforward with conventional sequences. But, arachnoid cysts, small colloid cysts, or obstructive membranes in the third ventricle require careful attention.

The cerebral aqueduct

In the proper clinical setting, in conjunction with the triventricular hydrocephalus, the absence of the flow void sign, and the normal-appearing fourth ventricle, it is usually

straightforward to point out the stenosis in the cerebral aqueduct. However, the diagnosis of aqueduct stenosis may not be so clear in every case because of various clinical, etiologic, and radiological features [20] (Figs. 14, 15, 16, 17, and 18). The heterogeneity of clinical presentation and wide anatomical variation in the cerebral aqueduct may make the proper diagnosis more complicated and difficult. Morphologic MRI examinations indicate direct or indirect signs suggesting aqueduct stenosis, but these signs have provided only subjective quantitative data. We suggest the complementary use of rapid and reproducible cine PC sequence through the cerebral aqueduct to prove the obstruction of CSF circulation at this level.
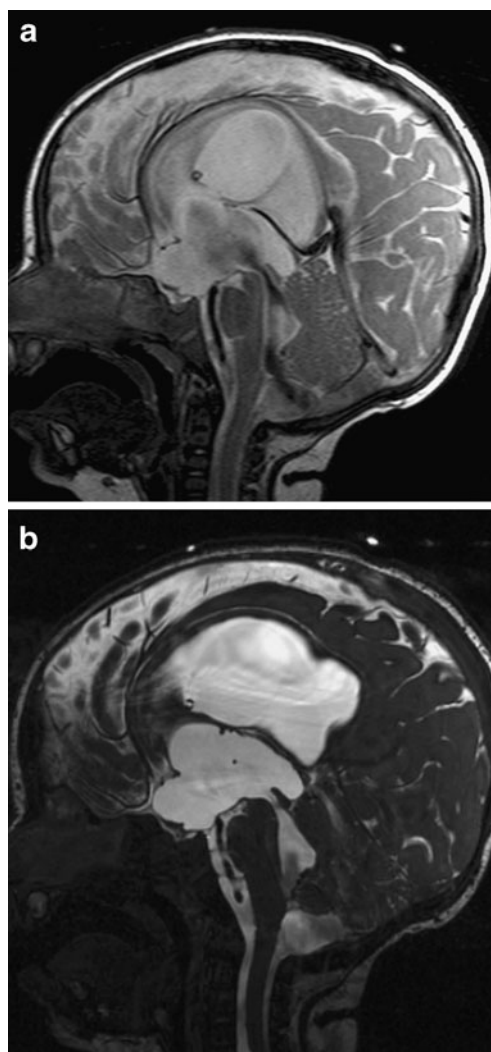
Fig. 19 Sagittal TSE T2 weighted image (a) of the patient with progressive head enlargement points out severe tetraventricular hydrocephalus. The cerebral aqueduct and foramen of Magendie seem to be open with extensive flow void phenomenon, but 3D CISS (b) nicely demonstrates an obstructive membrane in the foramen of Magendie

Fig. 20 Sagittal TSE T2 weighted image (**a**) and 3D CISS (**b**) images of the patient who had ETV and posterior fossa surgery exhibit tetraventricular hydrocephalus and syringomyelia in the cervical spinal cord. On sagittal TSE T2 weighted image, the stoma seems to be open, but not functional. 3D CISS image shed light on why the stoma is not functional, showing total obliteration in the prepontine cistern. Parasagittal 3D CISS image demonstrates obliteration in the foramen of Luschka (**c**). Sagittal cine PC obtained at systole (**d**) and diastole (**e**) confirms that there is not any CSF flow through the basal cisterns and midsagittal fourth ventricle exit
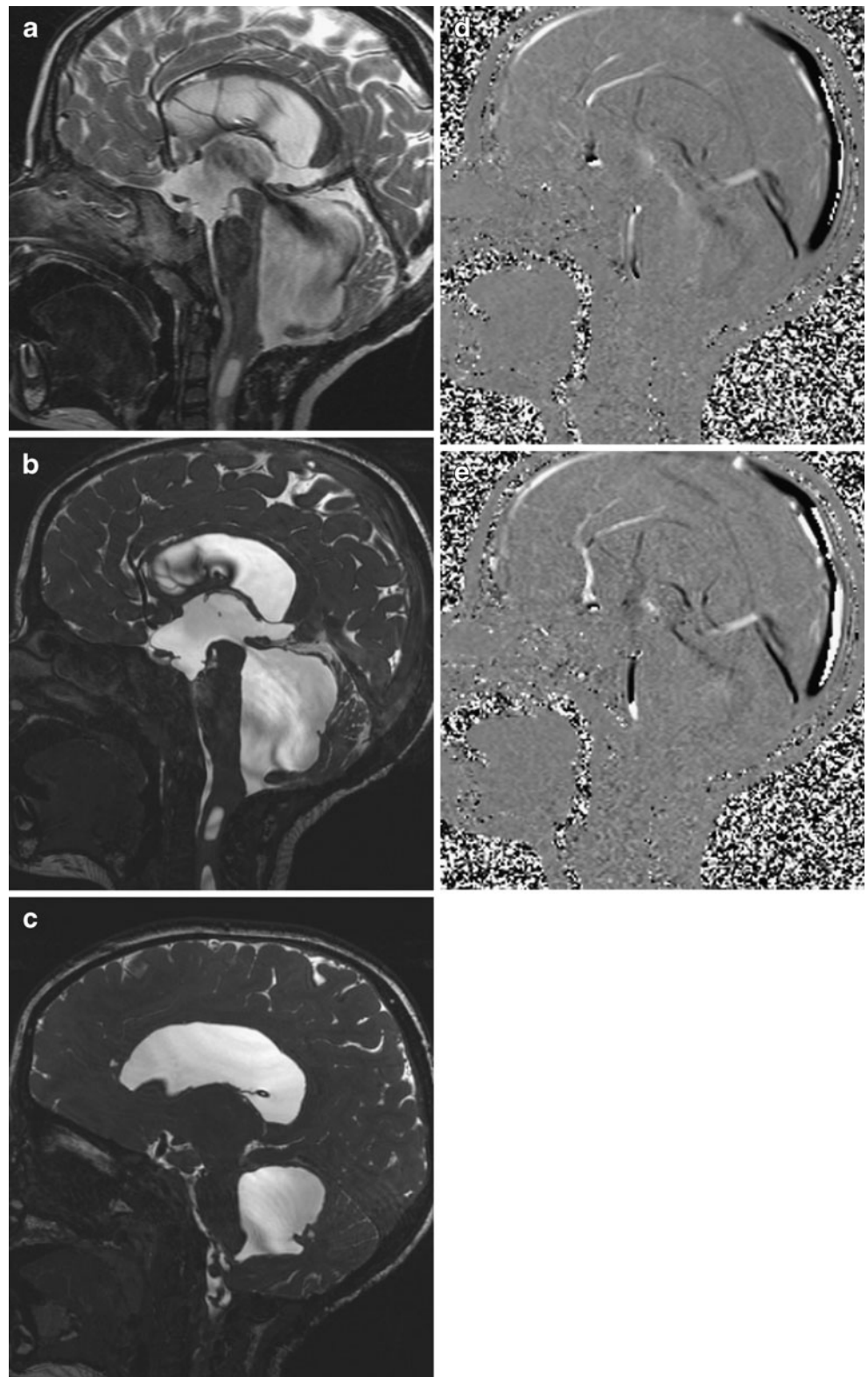
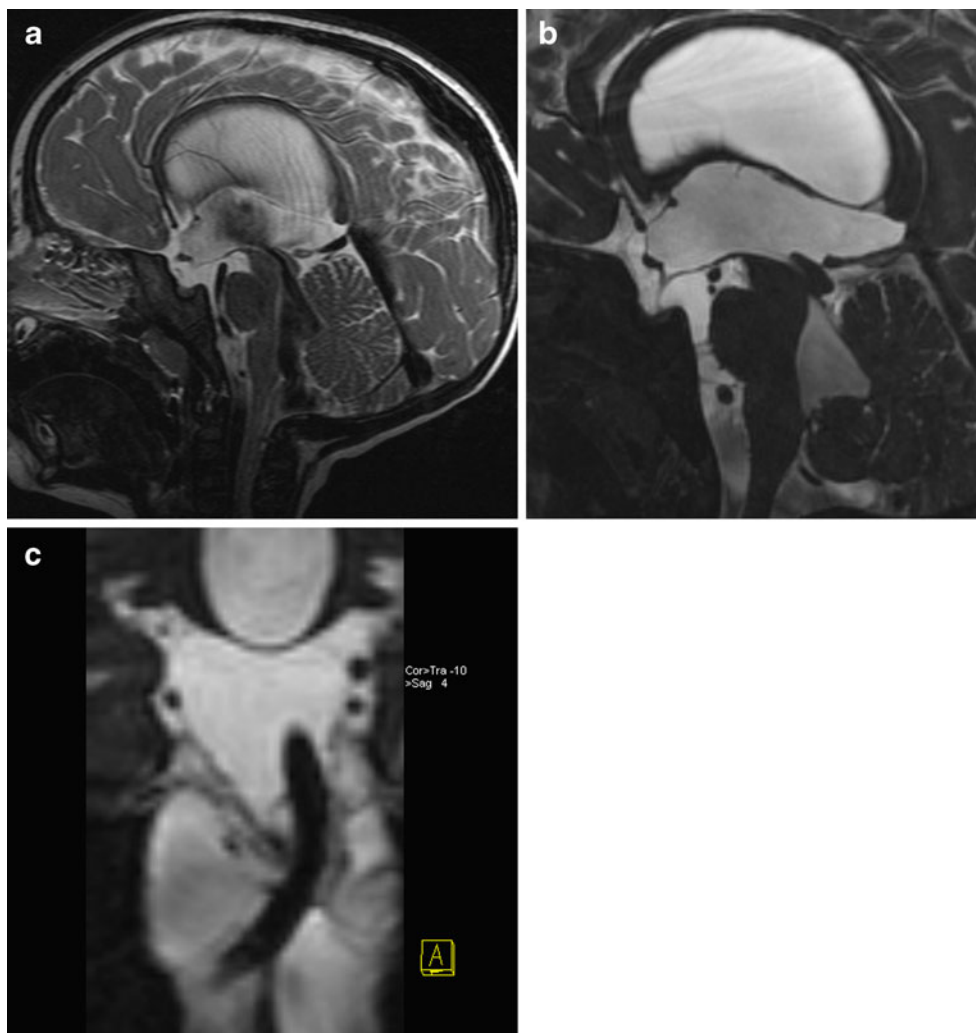## The fourth ventricle inlet and outlets

Neuroimaging should provide a diagnosis more than that of fourth ventricle tumors, posterior fossa arachnoid cysts, or

Dandy–Walker syndrome. Superior velum medullary synechia is usually presented with triventricular hydrocephalus, normal-sized fourth ventricle, and wide open cerebral aqueduct, simulating communicating hydrocephalus, but
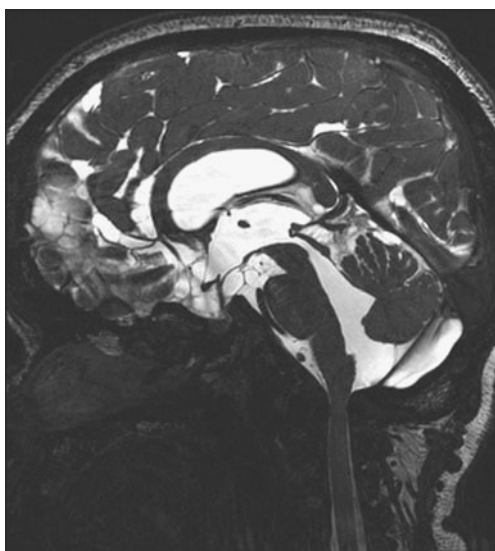
Fig. 21 Sagittal 3D CISS demonstrates mild to moderate hydrocephalus in a patient with achondroplasia. Liliequist membrane is seen below the floor of the third ventricle. There is not any other obstructive membrane in the cisterns and ventricles. However, foramen magnum is narrowed and the CSF space around the cervicomedullary junction is obliterated

Fig. 22 Sagittal TSE T2 weighted image (**a**) indicates tetraventricular hydrocephalus with extensive flow void in the cerebral aqueduct, in the fourth ventricle, and in the foramen of Magendie compatible with communicating hydrocephalus, but sagittal 3D CISS (**b**) and its coronal reformat (**c**) reveal the obstructive membrane in the prepontine cistern

careful assessments indicate lack of flow void in the cerebral aqueduct in the midsagittal TSE T2 weighted image and an obstruction of the fourth ventricle inlet in 3D CISS (Fig. 4). Cine PC could be used as a complimentary sequence to confirm the obstruction of the fourth ventricle inlet.

The radiological investigation of the fourth ventricle outlet has been unheeded due to low spatial resolution, poor tissue contrast, and flow-related artifact of conventional T1-weighted and T2-weighted sequences. Until recently, there has been no publication in terms of radiological demonstration of fourth ventricle outlet obstructions dealing with a clinical series more than a case report [6]. 3D CISS with real-time multiplanar reconstruction could easily demonstrate membranes which divide the cisterns and the fourth ventricle either in foramen of Magendie or foramina of Luschka or both (Figs. 5, 19, and 20).

Foramen magnum

A narrow foramen magnum is observed in several osteochondrodysplasias and metabolic disorders, such as

Fig. 23 Axial TSE T2 weighted image (**a**) through the lateral ventricles and midsagittal TSE T2 weighted image (**b**) show a supposed diagnosis of communicating hydrocephalus without any clue for obstruction. Sagittal 3D CISS (**c**) and its coronal reformat (**d**) indicate that there are thickened membranes in the horizontal, vertical, and oblique directions in the prepontine cistern. Sagittal cine PC obtained at systole (**e**) and diastole (**f**) represent biphasic flow in the cervical subarachnoid, cerebral aqueduct, and foramen of Magendie, but not in the prepontine cistern
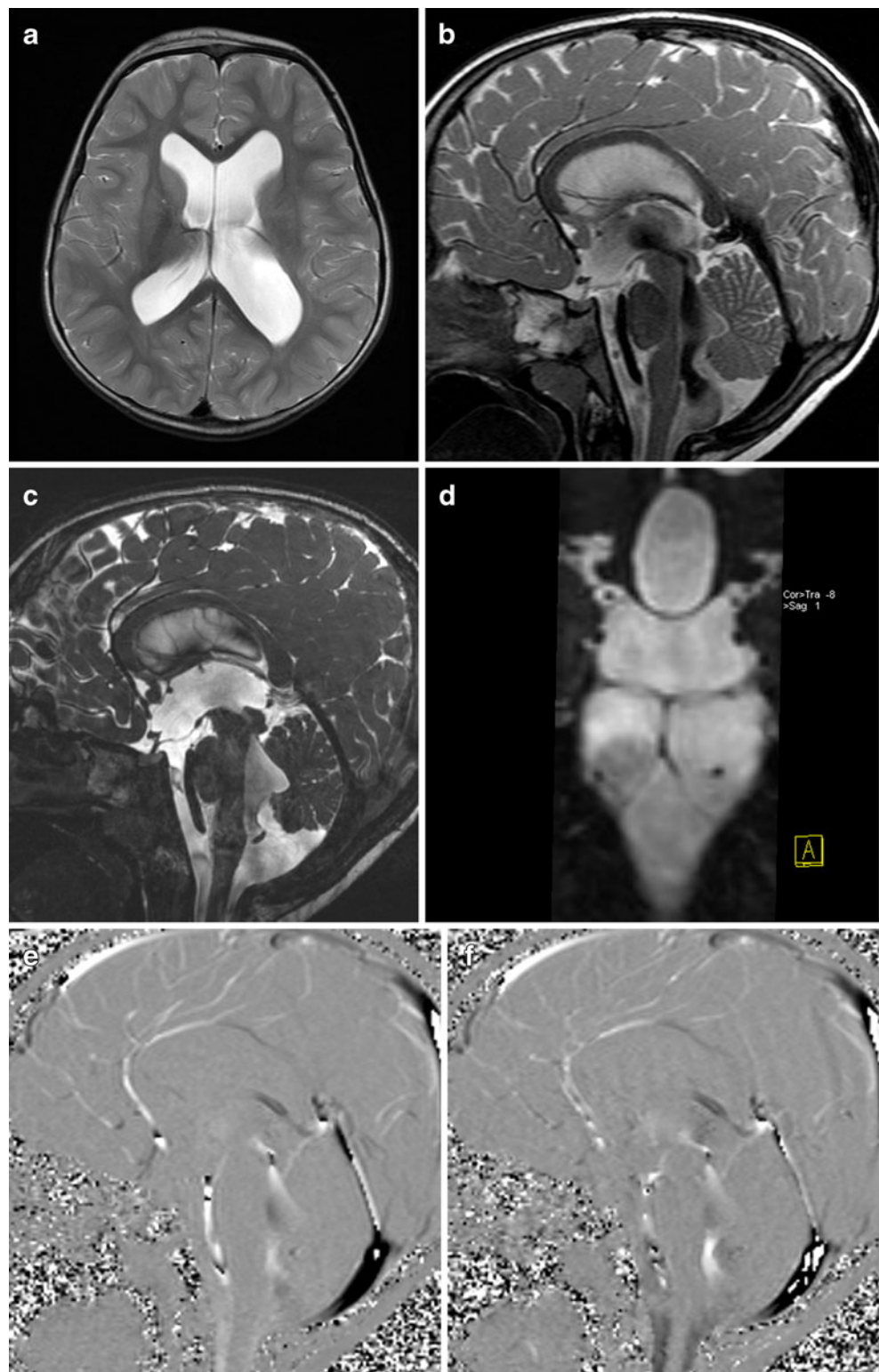

achondroplasia and mucopolysaccharidoses [19]. This osseous disease is complicated by obstruction of the cerebral venous return at the level of the jugular foramen. However, the pathophysiology of hydrocephalus is not clear in such osseous diseases. While morphologic imaging show the obliteration of the subarachnoid near the foramen magnum, cine PC demonstrates CSF flow disturbance at the craniocervical junction (Fig. 21).
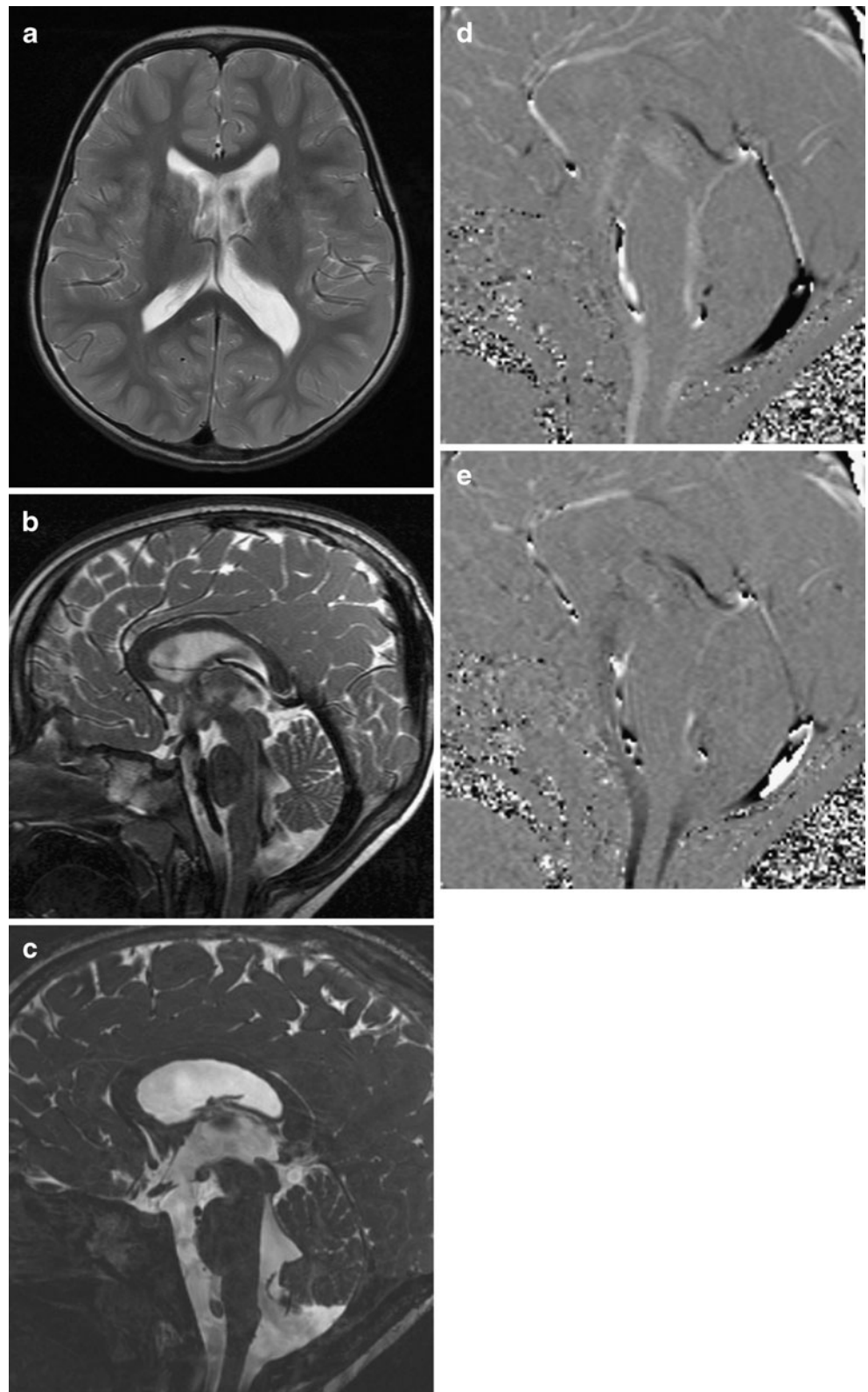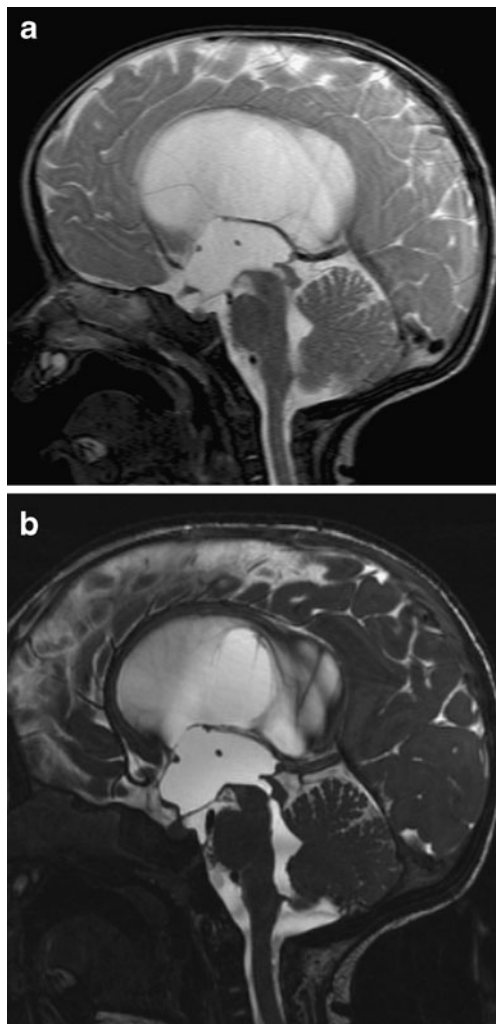
The basal cisterns

The basal cisterns are the major gateways for CSF to reach the cortical subarachnoid space. Blockage or resistance in these sites not only causes obstructive hydrocephalus but also affect the success of neuro-endoscopic procedures [2, 4, 14] (Figs. 22, 23, and 24).

Fig. 25 It is easy to depict a stenosis in the lower part of the cerebral aqueduct on sagittal TSE T2 weighted image (**a**), but there is no other clue for an obstruction in the other part of the CSF pathway. However, sagittal 3D CISS (**b**) represents obstructions not only in the cerebral aqueduct, but also in the foramen of Magendie and prepontine cistern

## Preoperative radiological assessment of endoscopic third ventriculostomy

Careful assessment with preoperative MRI is critical in order to avoid complications during surgery and to be able to achieve a good outcome. The anatomical details of related structures must be carefully evaluated. The size of the lateral ventricles and foramina of Monro, third ventricular width, and the position of basilar artery tip relative to the mammillary bodies, presence or absence of membranes in the ventricles and basal cisterns, and presence or absence of severe skull base anomaly should be documented. All possible membranes in ventricles and cisterns are carefully scrutinized by using 3D CISS with MPVR (Fig. 25). If needed, cine PC could be used to confirm the obstructive nature of membranes in the cisterns or ventricles.

Postoperative radiological assessment of ETV

MRI and CT criteria, such as demonstration of midsagittal surgical defect of the floor of the third ventricle, resolution of periventricular edema, widening of subarachnoid space, or diminish in ventricular size, which is used successfully to evaluate patients after shunt insertion, are unreliable in judging the patency of ventriculostomy fenestration [5]. So, functional analysis of ventriculostomy patency and the assessment of the procedural success mainly rely on the demonstration of flow void or flow signal in the floor of the
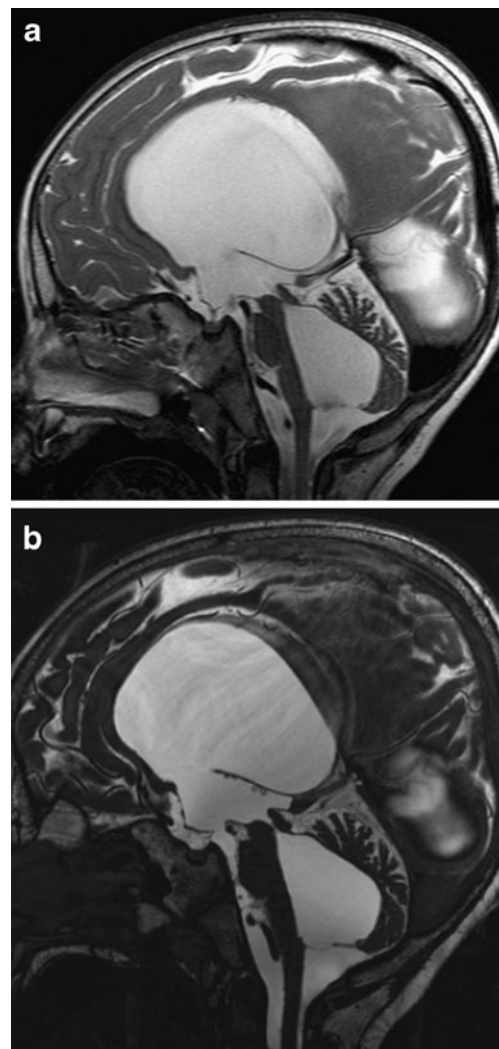
Fig. 26 At 12-month follow-up after ETV due to aqueduct stenosis, sagittal TSE T2 weighted image (**a**) shows an open stoma with subtle flow void through it. The aqueduct stenosis is depicted clearly on sagittal TSE T2 weighted image, but it is hard to say that there is a complete obliteration in the foramen of Magendie. The findings obtained from TSE T2 weighted image sequences could falsely conduct somebody as a functional stoma, but sagittal 3D CISS (**b**) indicates a trapped fourth ventricle and obliteration of the prepontine cistern. The stoma is open with little function due to extensive obstructive membranes in the prepontine cistern
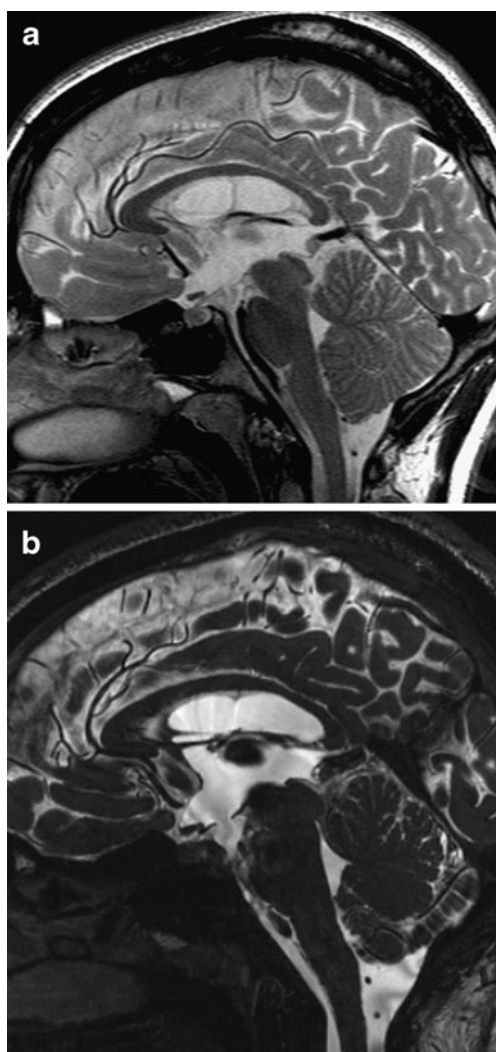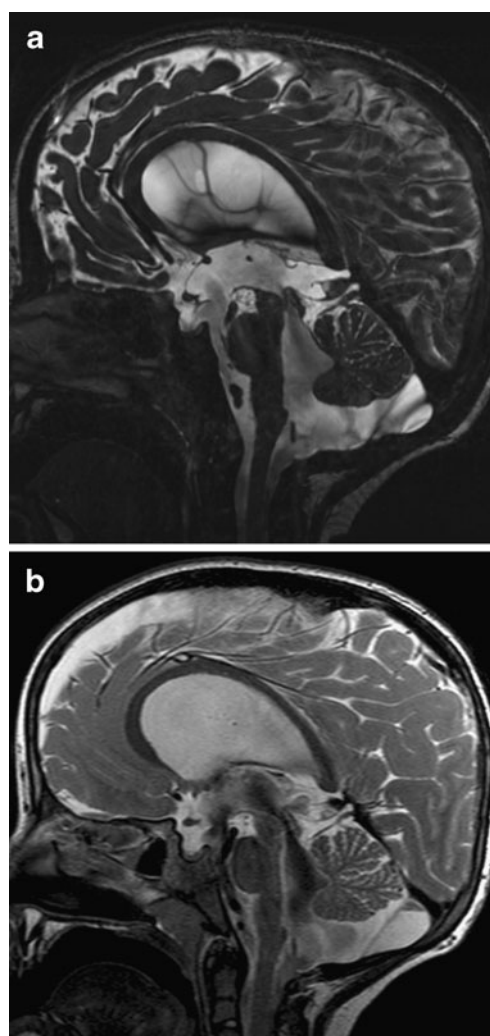
Fig. 27 Sagittal TSE T2 weighted image (**a**) nicely demonstrates an open stoma of the patient with ETV. Furthermore, lack of flow void through the stoma confirms the failed ETV, but it is not possible to say the cause of the failed ETV with TSE T2 weighted image sequence alone. However, sagittal 3D CISS (**b**) reveal the cause, pointing out the prepontine obstructive membranes

third ventricle by MRI [5] (Figs. 26, 27, and 28). Also, the triage of patients with failed endoscopic third ventriculostomy (ETV) solely depends on whether the stoma of ETV is functional or not, since the former requires shunt insertion, while the latter may be explored for redo ETV. Since the follow-up of patients with ETV rely mainly on demonstration of flow or flow void through the stoma, the methodology which is used to judge this finding has crucial importance. While various MRI sequences have been applied to solve this problem, TSE T2 weighted image and cine PC are most useful in the assessment of flow through the fenestration. However, the proper demonstration of flow through the fenestration with TSE T2 weighted image depends strongly on appropriate selection of se-

quence parameters and imaging planes [5]. Sagittal TSE T2 weighted image with 2-mm slice thickness provides prompt and robust qualitative evidence for the existence of flow through the fenestration [5]. If the findings of TSE are equivocal to demonstrate flow void adequately, both sagittal and oblique axial cine PC through the stoma could be used effectively with the proper sequence parameters [5]. While through plane axial cine PC could be assessed quantitatively to obtain stroke volume through the stoma, qualitative assessment of them in real-time cine mode is essential.

Conclusion

Neuroimaging has a key role in the treatment and follow-up of the patients with hydrocephalus since its beginnings.

Fig. 28 At 6-month follow-up of a patient after ETV, sagittal 3D CISS (**a**) indicates an open stoma with clear cisterns, but it is hard to say if the stoma is functional or not. However, sagittal TSE T2 weighted image (**b**) reveals marked CSF flow void through the stoma, representing proper function

Furthermore, neuroendoscopic procedures have increased the demands from neuroimaging. If neuroendoscopic procedures are available as a treatment option, US and CT are far from meeting expectations. MRI is the single modality to support both anatomical and functional information which address all the problems. Furthermore, there is no other option in the follow-up of the patients after neuroendoscopic procedures such as ETV. But, a more sophisticated MRI approach rather than a routine cranial MRI, combining various MRI sequences, is needed to fulfill the necessary requirements.

References

1. Aleman J, Jokura H, Higano S, Akabane A, Shirane R, Yoshimoto T (2001) Value of constructive interference in steady-state three-dimensional, Fourier transformation magnetic resonance imaging for the neuroendoscopic treatment of hydrocephalus and intracranial cysts. Neurosurgery 48:1291–1295, discussion 1295–1296

2. Anik I, Ceylan S, Koc K, Anik Y, Etus V, Genc H (2011) Membranous structures affecting the success of endoscopic third ventriculostomy in adult aqueductus sylvii stenosis. Minim Invasive Neurosurg 54:68–74

3. Bartelt D, Jordan CE, Strecker EP, James AE (1975) Comparison of ventricular enlargement and radiopharmaceutical retention: a cisternographic–pneumoencephalographic comparison. Radiology 116:111–115

4. Dincer A, Yener U, Ozek MM (2011) Hydrocephalus in patients with neurofibromatosis type 1: MR imaging findings and the outcome of endoscopic third ventriculostomy. AJNR Am J Neuroradiol 32:643–646

5. Dincer A, Yildiz E, Kohan S, Memet Ozek M (2011) Analysis of endoscopic third ventriculostomy patency by MRI: value of different pulse sequences, the sequence parameters, and the imaging planes for investigation of flow void. Childs Nerv Syst 27:127–135

6. Dincer A, Kohan S, Ozek MM (2009) Is all "communicating" hydrocephalus really communicating? Prospective study on the value of 3D-constructive interference in steady state sequence at 3 T. AJNR Am J Neuroradiol 30:1898–1906

7. Doll A, Christmann D, Kehrli P, Abu Eid M, Gillis C, Bogorin A, Thiebaut A, Dietemann JL (2000) Contribution of 3D CISS MRI for pre- and post-therapeutic monitoring of obstructive hydrocephalus. J Neuroradiol 27:218–225

8. Drayer BP, Rosenbaum AE, Reigel DB, Bank WO, Deeb ZL (1977) Metrizamide computed tomography cisternography: pediatric applications. Radiology 124:349–357

9. Greitz D (2004) Radiological assessment of hydrocephalus: new theories and implications for therapy. Neurosurg Rev 27:145–165, discussion 166–147

10. Guillaume DJ (2010) Minimally invasive neurosurgery for cerebrospinal fluid disorders. Neurosurg Clin N Am 21:653–672, vii

11. James AE Jr, New PF, Heinz ER, Hodges FJ, DeLand FH (1972) A cisternographic classification of hydrocephalus. Am J Roentgenol Radium Ther Nucl Med 115:39–49

12. Kim DS, Choi JU, Huh R, Yun PH, Kim DI (1999) Quantitative assessment of cerebrospinal fluid hydrodynamics using a phase-contrast cine MR image in hydrocephalus. Childs Nerv Syst 15:461–467

13. Kurihara N, Takahashi S, Tamura H, Higano S, Furuta S, Jokura H, Umetsu A (2000) Investigation of hydrocephalus with three-dimensional constructive interference in steady state MRI. Neuroradiology 42:634–638

14. Laitt RD, Mallucci CL, Jaspan T, McConachie NS, Vloeberghs M, Punt J (1999) Constructive interference in steady-state 3D Fourier-transform MRI in the management of hydrocephalus and third ventriculostomy. Neuroradiology 41:117–123

15. Oertel JM, Mondorf Y, Schroeder HW, Gaab MR (2010) Endoscopic diagnosis and treatment of far distal obstructive hydrocephalus. Acta Neurochir (Wien) 152:229–240

16. Oi S, Di Rocco C (2006) Proposal of "evolution theory in cerebrospinal fluid dynamics" and minor pathway hydrocephalus in developing immature brain. Childs Nerv Syst 22:662–669

17. Rekate HL (2008) The definition and classification of hydrocephalus: a personal recommendation to stimulate debate. Cerebrospinal Fluid Res 5:2

18. Rekate HL (2009) A contemporary definition and classification of hydrocephalus. Semin Pediatr Neurol 16:9–15

19. Rollins N, Booth T, Shapiro K (2000) The use of gated cine phase contrast and MR venography in achondroplasia. Childs Nerv Syst 16:569–575, discussion 575–567

20. Stoquart-El Sankari S, Lehmann P, Gondry-Jouet C, Fichten A, Godefroy O, Meyer ME, Baledent O (2009) Phase-contrast MR imaging support for the diagnosis of aqueductal stenosis. AJNR Am J Neuroradiol 30:209–214

21. Tondreau RL (1985) The retrospectoscope. Egas Moniz 1874–1955. Radiographics 5:994–997

22. van Lindert EJ, Beems T, Grotenhuis JA (2006) The role of different imaging modalities: is MRI a conditio sine qua non for ETV? Childs Nerv Syst 22:1529–1536